Combustion and Flame 256 (2023) 112986

Contents lists available at ScienceDirect

Combustion and Flame

journal homepage: www.elsevier.com/locate/combustflame

Intrinsic instabilities of hydrogen and hydrogen/ammonia premixed flames: Influence of equivalence ratio, fuel composition and pressure

Jessica Gaucherand[a,b,*], Davide Laera[b,c], Corinna Schulze-Netzer[a], Thierry Poinsot[b,d]

[a] Department of Energy and Process Engineering, Norwegian University of Science and Technology, Trondheim NO-7034, Norway
[b] CERFACS, 42 avenue Gaspard Coriolis, Toulouse 31057, France
[c] Department of Mechanics, Mathematics and Management, Polytechnic University of Bari, Via Orabona 4, Bari 70125, Italy
[d] IMFT, Allée du Professeur Camille Soula, Toulouse 31400, France

ARTICLE INFO

Article history:
Received 1 March 2023
Revised 18 July 2023
Accepted 20 July 2023

Keywords:
Direct numerical simulation
Ammonia and hydrogen
Dispersion relation
Premixed flame
Thermo-diffusive instabilities

ABSTRACT

Premixed lean hydrogen-air flames exhibit instabilities due to hydrodynamic instabilities but also thermo-diffusive instabilities. However, in the case of ammonia/hydrogen blends, the effect of ammonia addition on instabilities is still unclear. To investigate intrinsic instabilities in premixed ammonia/hydrogen-air flames, a parametric study of laminar premixed flames is performed for different fuel contents, from pure hydrogen (H_2) to a blend of 40% of H_2 and 60% of ammonia (NH_3) in volume, equivalence ratios (0.4 to 1.0) and pressures (1 and 10 bar) to investigate thermo-diffusive instabilities. Numerical simulations using detailed chemistry are performed where an initial perturbation is set to disturb the planar flame front and to compute its growth rate. During the initial linear phase, the perturbation's amplitude grows or decreases depending on the flame's mixture propensity to be unstable or stable, respectively. At small times, the linear growth rate of the perturbation can be estimated and compared to theory. As expected, the maximum growth rate obtained in the linear phase depends on the mixture's equivalence ratio, fuel ratio, and pressure. Ammonia addition leads to a reduced peak growth rate, likely due to lower reactivity leading to a higher Zel'dovich number. Very lean mixtures (equivalence ratios of 0.4 and 0.5) are thermo-diffusively unstable, regardless of the ammonia content, due to hydrogen's preferential diffusion.

1. Introduction

Carbon-free fuels have recently been of interest to decarbonize energy systems such as gas turbines, internal combustion engines, boilers and furnaces [1]. Indeed, these fuels, such as hydrogen (H_2) or ammonia (NH_3) emit no CO or CO_2 as they burn with air. However, their introduction in combustors remains a challenge. Indeed, H_2 has a considerable flame speed and wide flammability range, not only requiring the redesign of chambers but also, raising safety issues [2]. Storage and transportation difficulties are also expected from the volatility and low volumetric energy density of H_2. On the other hand, while NH_3 is easier to store and transport [3], it is characterized by a very low flame speed which limits its direct use in combustion systems. This major drawback can be offset by mixing NH_3 with H_2: research has shown the potential of mixing these two fuels to find a compromise in terms of each fuel's advantages and drawbacks [4,5].

To implement H_2 and NH_3 mixtures as fuels at a large scale, a fundamental understanding of the flame front structures and propagation is necessary. Experimental and numerical works have highlighted the effect of preferential diffusion in lean H_2 flames, leading to thermo-diffusive instabilities [6,7]. These flames are characterized by significant wrinkling, enhanced speed, and shortened length. Thermo-diffusive instabilities have been experimentally studied in different setups such as laminar and turbulent spherical flames [8], fan-stirred chamber and coflow jets at high Reynolds number [9]. Numerically, direct numerical simulations (DNS) are often used to investigate such phenomena. Lean H_2-air premixed flames have been investigated using DNS, showing that thermo-diffusive effects strongly affected the flame [10,11]. These studies showed that models for turbulent premixed flame need to account for thermo-diffusive effects at two levels:

- locally, along the flame front, each unit surface of the flame can burn, on average, more than the laminar-unstrained flame speed, S_L^0. This can be measured through an indicator I_0 defined

* Corresponding author at: Department of Energy and Process Engineering, Norwegian University of Science and Technology, Trondheim NO-7034, Norway.
E-mail address: gaucherand@cerfacs.fr (J. Gaucherand).

https://doi.org/10.1016/j.combustflame.2023.112986

by the normalized, surface averaged consumption speed along the front:

$$I_0 = \frac{< s_c >}{s_L^0}. \quad (1)$$

- Cells are formed on the flame front, independently of any wrinkling due to turbulent eddies. This wrinkling due to thermo-diffusive effects is called Θ_0 and is defined by:

$$\Theta_0 = \frac{\Sigma}{L_x}. \quad (2)$$

where Σ is the flame surface and L_x the reference or initial flame surface.

The overall effects of thermo-diffusive instabilities are measured by the product $I_0\Theta_0$ which indicates the factor by which the total reaction rate increases. Values of $I_0\Theta_0$ up to 4 have been reported by Berger et al. for a turbulent lean H_2-air flame at equivalence ratio $\phi = 0.4$ [10]. $I_0\Theta_0$ up to six were observed experimentally for premixed turbulent spherical H_2-air flames while $I_0\Theta_0$ for CH_4 flames were close to unity [8]. Increasing the pressure also increases $I_0\Theta_0$ as demonstrated for a premixed turbulent H_2-air at $\phi = 0.7$ for pressures going from 1 to 7 bar [12].

Preferential diffusion effects have also been observed for premixed turbulent $NH_3/H_2/N_2$-air (40% NH_3, 45% H_2, and 15% N_2 in the fuel) flames at $\phi = 0.45$ with $I_0\Theta_0$ above 1.5 [13]. On the other hand, at $\phi = 1$, for a premixed turbulent NH_3/H_2-air flame (54% NH_3, and 46% H_2), unity $I_0\Theta_0$ values were found [14]. Rieth et al. [15] also found enhanced effects, at high pressure, of molecular hydrogen diffusion in leading points for premixed $NH_3/H_2/N_2$-air when comparing initial pressures at 1 bar and 10 bar. These results indicate that equivalence ratio, fuel and composition (in the case of blends), and initial pressure affect the development of thermo-diffusive instability.

A simple solution to predict the occurrence of thermo-diffusive instabilities would be to rely on theory [16–18]. Theoretical analyses of these instabilities have been carried out for decades for laminar premixed flames undergoing a small perturbation. Matalon and Matkowsky assumed a global one-step reaction [16] for Lewis close to unity, and Sivashinsky considered a small density jump throughout the flame front but accounted for a small Lewis number [19,20]. Recently, Berger et al. [21] have shown that these theories do not accurately capture the evolution of lean premixed H_2-air flames [21]. Accounting for fuel mixtures and complex chemistry is another difficulty. This is where simulations can be introduced: a stability analysis can be performed using 2-D DNS, where a planar flame is exposed to a small perturbation. During the first instants, also called the linear phase, the perturbation's amplitude will either grow or decrease: the growth rate of a given wavelength can be evaluated to reconstruct a dispersion relation [21,22]. This dispersion relation quantifies the stability of a given mixture.

Numerical studies of dispersion relations have been carried out using DNS by Berger et al. [21] in a parametric study to investigate premixed H_2-air flames by varying the equivalence ratio, initial pressure, and temperature using detailed chemistry. Detailed chemistry was also used by Altantzis et al. [23] to study lean premixed H_2-air at $\phi = 0.6$ and 5 atm for different domain lengths. Frouzakis et al. [22] studied H_2-air for $0.5 \leq \phi \leq 2.0$ and found good agreement of theoretical dispersion relation for $\phi \geq 0.75$. Yuan et al. [24] used one-step chemistry to simulate flames with unity Lewis numbers to study the effect of increasing pressure up to 5 bar. Higher pressure was investigated by Yu et al. [25] for a premixed H_2-air flame at $\phi = 0.6$ who found enhanced hydrodynamic instabilities for high-pressure cases. Studies have highlighted preferential diffusion in premixed NH_3/H_2-air flame experimentally in expanding spherical flames [26,27]. Dampened thermo-diffusive instabilities were observed qualitatively in lean conditions (up to $\phi = 0.6$) when increasing the amount of NH_3 [26] in NH_3/H_2 mixtures. However, increasing the initial pressure destabilized NH_3/H_2-air flames at $\phi = 0.8$ and $\phi = 1.0$ [27]. However, to the authors' knowledge, no dispersion relation has been computed yet for NH_3/H_2-air flames and compared to theoretical relations. In fact, due to the large difference between the Lewis number of the two fuels, as well as the possible dissociation of ammonia into hydrogen for intermediate temperature, the question of whether ammonia addition will dampen the instabilities is an open one with no definitive answer. Notably, some research has highlighted a non-monotonic evolution of the Markstein number for fixed equivalence ratio and varying H_2 content in NH_3/H_2 mixtures [28,29]. Therefore, several hypotheses can be formulated about what the effect of ammonia addition to hydrogen might lead to: 1) NH_3 dissociating into H_2 at intermediate temperature could lead to more instabilities, 2) H_2 could dominate the flame front destabilization and the NH_3/H_2 flame might behave like a pure H_2 flame, 3) or NH_3 addition might dampen the instabilities.

The present work aims to fill the literature gap by providing growth rate values for an extensive range of mixtures, varying equivalence ratios, and fuel composition from pure hydrogen to mixtures of ammonia and hydrogen up to 60% of ammonia in volume. The effect of pressure on instabilities will also be investigated for cases at $\phi = 0.5$ for pure H_2 and for a blend of 50% of NH_3 and H_2 in volume. DNS using detailed chemistry will provide quantitative information on the strength of thermo-diffusive instabilities for these mixtures, to be compared with theory. Thermo-diffusive instabilities will also be compared to hydrodynamic instabilities to investigate if NH_3/H_2-air flames can be thermo-diffusively unstable, how does NH_3 affects the flame stability, and how high pressure affects NH_3/H_2 flames. These will provide useful insights on the mixtures' impact on thermo-diffusive instabilities, which is needed for the combustion model development for ammonia/hydrogen and supports the fuel blend selection for retrofitting. Section 2 covers the theoretical dispersion relation formulas, the numerical setup, the parametric variations performed, and the methodology to compute the numerical relation dispersion. Section 3.1 presents the results obtained for the numerical dispersion relation, Section 3.2 presents expressions for the Lewis number of NH_3/H_2 blends which are then used in Section 3.3 to compare the dispersion relation from the DNS results with theoretical predictions [16,19,30]. The impact of other global flame parameters is also investigated in Section 3.4, and a fit of the peak growth rate based on the DNS data is provided in Section 3.5 before concluding in Section 4.

2. Theory, numerical setup and methodology to compute the flame growth rate

2.1. Theoretical background of flame response to perturbation

Works by Darrieus and Landau [30,31] showed how planar flames were intrinsically unstable due to hydrodynamic instabilities caused by the density jump in the flame front from fresh to burned gases. The hydrodynamic instability ω_{DL} can be defined as:

$$\omega_{DL} = \frac{\sqrt{\sigma^3 + \sigma^2 - \sigma} - \sigma}{\sigma + 1}, \quad (3)$$

where $\sigma = \frac{\rho_u}{\rho_b}$ is the expansion ratio equal to unburned over burned density. The non-dimensional growth rate $\bar{\omega}$ dependency with respect to non-dimensional wave number $\bar{k}$ can be written in a first estimation as :

$$\bar{\omega} = \omega_{DL}\bar{k}, \quad (4)$$

where $\bar{\omega} = \omega\tau$ and $\bar{k} = k\delta_L^0$. The flame time τ corresponds to the ratio of the flame thermal thickness δ_L^0 to the unstretched flame

speed s_L^0 and the thermal thickness δ_L^0 is defined by :

$$\delta_L^0 = \frac{T_{ad} - T_u}{\max(\nabla T)}, \tag{5}$$

where T_u is the initial flame temperature, and T_{ad} is the adiabatic flame temperature. However, numerical and experimental work have not observed this unconditional instability, and Eq. (4) is incomplete. New dispersion relations have been derived, such as the one by Matalon et al. [16] where a second-order term is added to account for a stabilizing or destabilizing behavior due to Lewis number effects:

$$\bar{\omega} = \omega_{DL}\bar{k} - \delta\left[B_1 + \beta\left(Le_{eff} - 1\right)B_2 + P_r B_3\right]\bar{k}^2 = \omega_{DL}\bar{k} - \omega_2\bar{k}^2. \tag{6}$$

The diffusive flame thickness $\delta_D = D_{th}/s_L^0$, where D_{th} is the thermal diffusivity, is needed to define $\delta = \delta_D/\delta_L^0$. The coefficients B_1, B_2, and B_3 are functions of the expansion ratio, the thermal conductivity evolution with temperature, and ω_{DL} [32]:

$$B_1 = \frac{\sigma}{2\left(\sigma + (\sigma+1)\omega_{DL}\right)}\left(\frac{\sigma(2\omega_{DL}+\sigma+1)}{\sigma-1}\int_1^\sigma \frac{\bar{\lambda}(x)}{x}\mathrm{d}x + \int_1^\sigma \bar{\lambda}(x)\mathrm{d}x\right), \tag{7}$$

$$B_2 = \frac{\sigma(1+\omega_{DL})(\sigma+\omega_{DL})}{2(\sigma-1)\left(\sigma+(\sigma+1)\omega_{DL}\right)}\int_1^\sigma \log\left(\frac{\sigma-1}{x-1}\right)\frac{\bar{\lambda}(x)}{x}\mathrm{d}x, \tag{8}$$

$$B_3 = \frac{\sigma}{\sigma+(\sigma+1)\omega_{DL}}\left((\sigma-1)\bar{\lambda}(\sigma) - \int_1^\sigma \bar{\lambda}(x)\mathrm{d}x\right), \tag{9}$$

where $\bar{\lambda} = \lambda/\lambda_u$ is the normalised thermal conductivity and $x = T/T_u$.

The Prandtl number P_r, the Zel'dovich number β, and the effective Lewis number Le_{eff} are also needed in Eq. (6). Zel'dovich number β for detailed chemistry is computed using the approach proposed by Law et al. [33] to evaluate the overall activation energy:

$$\frac{E_a}{R} = -2\frac{\mathrm{d}\left(\rho_u S_L^0\right)}{\mathrm{d}(1/T_{ad})}, \tag{10}$$

where R is the universal gas constant. To vary the adiabatic temperature and calculate Eq. (10), two 1-D flames are computed where the amount of N_2 is varied slightly (±0.3%). The overall activation energy is computed with the gradient of the line obtained using a linear fit of the curve given by plotting $\rho_u S_L$ over $1/T_{ad}$, using the results of the two 1-D flames. The values of E_a used in this work are provided in the Supplementary Material in Fig. C.1. The Zel'dovich number β is given by:

$$\beta = \frac{E_a(T_{ad} - T_u)}{RT_{ad}^2}. \tag{11}$$

Matalon et al.'s dispersion relation Eq. (6) is derived for Lewis numbers close to unity, where the second term of the expression ω_2 has a stabilizing effect. However, for lower values of Lewis number, ω_2 is positive: the dispersion relation becomes destabilizing for all wave numbers. Sivashinsky [19,20] derived a dispersion relation for the linear phase accounting for a fourth-order term that is stabilizing regardless of the Lewis number:

$$\bar{\omega} = \delta\left[\frac{\beta}{2}(1-Le) - 1\right]\bar{k}^2 - 4\delta^3\bar{k}^4. \tag{12}$$

Another relation by Sivashinsky was derived for the non-linear flame evolution but is outside the scope of this work [34].

Further dispersion relations have been established by Pelce and Clavin [17], Klimenko and Class [35], Chung and Law [36] and others. Lipatnikov and Chomiak [37] reviewed the assumptions needed to derive dispersion relations and presented different theoretical relations, but the scope of our study will be limited to the theories of Darrieus-Landau (Eq. (4)), Matalon et al. (Eq. (6)), and Sivashinsky's (Eq. (12)) dispersion relations for comparison in Section 3.3.

A critical parameter in all theoretical evaluations of $\bar{\omega}$ is the effective Lewis number Le_{eff}. Defined by Joulin and Mitani [38] for two reactant flames, Le_{eff} is given by:

$$Le_{eff} = \begin{cases} \frac{Le_O + A Le_F}{1+A}, & A = 1 + \beta\left(\phi^{-1} - 1\right) \quad \text{if } \phi < 1, \\ \frac{Le_F + A Le_O}{1+A}, & A = 1 + \beta(\phi - 1) \quad \text{if } \phi > 1, \end{cases} \tag{13}$$

where Le_F and Le_O are the fuel's and oxidant's Lewis numbers. Oxygen O_2 is taken as the oxidant. When only one fuel is considered, the effective Lewis number is straightforward to derive, using the fuel's Lewis number in Eq. (13) (i.e in the case of pure H_2). However, for a fuel mixture, the fuel's Lewis number requires a new evaluation. Several definitions have been suggested and validated against experiment [39,40]. Three of them have been considered here. The first one (Le_V) was proposed by Muppala et al. [41], who suggested a volume-based formulation of the fuel's Lewis number (Le_V), based on the volume fraction (X_i) of each fuel in the fuel mixture:

$$Le_V = \sum_{n=1}^{f} X_i Le_i, \tag{14}$$

with f the number of fuels in the fuel mixture. Dinkelacker et al. [42] proposed a diffusion-based (Le_D) formula:

$$\frac{1}{Le_D} = \sum_{n=1}^{f} \frac{X_i}{Le_i}. \tag{15}$$

Law et al. [43] used a heat release-based formulation (Le_Q), where the Lewis number of each fuel is weighted by the nondimensional heat release (q_i) based on the consumption of each fuel:

$$Le_Q = 1 + \frac{\sum_{n=1}^{f} q_i(Le_i - 1)}{\sum_{n=1}^{f} q_i}, \tag{16}$$

with

$$q_i = \frac{Q_i Y_{i,u}}{C_p T_u}, \tag{17}$$

where Q_i is the heat of reaction of the fuel i and $Y_{i,u}$ its mass fraction far upstream. In the case of NH_3/H_2-air flames, Zitouni et al. [29] found that the Le_V definition matched their experimental results quite well, that the Le_D formulation was more suited for lean mixtures, and Le_Q was accurate in richer conditions. In this study, an analysis of strained flame will be performed to determine the most suited definition for the Lewis number in Section 3.2 and will be used to compute the theoretical dispersion relations discussed in Section 3.3. This comes as an addition to the scarce literature on the topic of a suited Lewis number definition for mixtures of ammonia and hydrogen.

2.2. Numerical setup

The reacting Navier–Stokes equations are solved with the compressible solver AVBP[1] [44], an explicit massively parallel code solving the conservation of mass, momentum, energy equations, and species transport. The flow is gaseous and NH_3/H_2-air chemistry is modeled using an analytically reduced chemistry mechanism derived from CRECK [45] and reduced with Arcane [46] (18 species, 6 species with QSS assumption and 150 reactions). Validation of the mechanism is presented in the Supplementary Materials in Fig. A.1. The reduced mechanism is also included in the Supplementary Materials. A power law is used to compute the molecular viscosity $\mu = \mu_{ref}(T/T_{ref})^b$. Constant Schmidt S_c and Prandtl

[1] http://www.cerfacs.fr/avbp7x.

Table 1
Overview of the 2-D DNS. For each case, the content of ammonia in volume in the fuel X_{NH_3}, the equivalence ratio ϕ, the initial pressure P, the laminar flame speed s_L^0, the thermal flame thickness δ_L^0, the diffusive flame thickness δ_D and the adiabatic temperature T_{ad} are provided.

Case name	X_{NH_3} [%]	ϕ [−]	P [bar]	s_L^0 [m/s]	δ_L^0 [μm]	δ_D [μm]	T_{ad} [K]
NH3-00-Phi-04	0	0.4	1	0.25	562	105	1416
Ref	0	0.5	1	0.56	382	49	1625
NH3-00-Phi-1	0	1.0	1	2.27	326	14	2242
NH3-03-Phi-04	30	0.4	1	0.07	1389	366	1343
NH3-03-Phi-05	30	0.5	1	0.19	686	139	1534
NH3-03-Phi-1	30	1.0	1	0.93	317	31	2222
NH3-05-Phi-04	50	0.4	1	0.02	3840	1187	1316
NH3-05-Phi-05	50	0.5	1	0.09	1277	307	1502
NH3-05-Phi-1	50	1.0	1	0.46	432	61	2169
NH3-06-Phi-04	60	0.4	1	0.01	8493	2657	1301
NH3-06-Phi-05	60	0.5	1	0.05	1983	506	1487
NH3-06-Phi-1	60	1.0	1	0.31	576	89	2147
NH3-00-Phi-05-10-bar	0	0.5	10	0.15	80	18	1633
NH3-05-Phi-05-10-bar	50	0.5	10	0.01	1099	60	1513

P_r numbers are used for species molecular diffusion: $D_k = \mu/S_{c_k}$, for species k, and for thermal conductivity: $\lambda = \mu C_p/P_r$ with C_p the specific heat capacity of the mixture. In the Supplementary Materials, a comparison between constant Lewis number assumption and varying Lewis number is illustrated for the reference case, with an overall good agreement, leading to the validity of the constant Lewis number assumption in these premixed flames.

The numerical scheme used to solve the equations is Lax–Wendroff [47], a second-order scheme in space and time. A third-order accurate in space and time Taylor–Galerkin finite-element scheme was also tested with no major difference, therefore the second-order scheme was used in the parametric study to save computational time. Simulations are performed in 2-D rectangular domains with length L_x and height L_y. Cartesian meshes are used to discretize the domain with the selected cell size to have 40 grid points in the thermal flame thickness δ_L^0. At the inlet (bottom of the rectangular domain), fresh gases are injected at a velocity equal to the laminar flame speed of the mixture computed with Cantera [48]. The flow exits the domain at the outlet (top of the rectangular domain), where static pressure is imposed. Inlet and outlet use non-reflecting NSCBC boundary conditions [49]. Periodic conditions are imposed in the spanwise direction x. Initially, the flame front is mapped onto the domain using a 1D flame computed with Cantera and is perturbed with a sinusoidal perturbation $F(x)$:

$$F(x) = A_0 \sin(kx), \tag{18}$$

with A_0 the initial amplitude of the perturbation, selected to be 2% of δ_L^0 (to remain in the linear regime), and k is the wave number of the perturbation. L_x is selected to be equal to the wavelength of the imposed perturbation: $\lambda = 2\pi/k = 2\pi/n\delta_L^0$, with n varying between 1 and 60. L_y corresponds to $24\delta_L^0$, and the initial perturbation is imposed at $18\delta_L^0$ in the y-axis (Fig. 1(a)).

An initial temperature T_u of 300K is selected for all conditions. The reference case is set for pure hydrogen at $\phi = 0.5$ at atmospheric pressure to compare the results with literature data and validate the methodology. Parametric variations of the equivalence ratio from $\phi = 0.4$ to 1 are performed. A parametric variation of ammonia concentration in the fuel composition from X_{NH_3}= 0% to 60% in volume is also performed. Some fuel blends are selected to be computed at 10 bar to study the effect of pressure at $\phi = 0.5$. An overview of the 14 simulations performed is presented in Table 1.

2.3. Methodology for growth rate computation

The early flame propagation is investigated to compute the dispersion relation. Below a critical wave number k_c, the flame front perturbation will either grow or decrease exponentially with time. The growth rate is computed with the flame front's amplitude evolution, tracked using the isoline $T = 3T_u$ to define the flame front. The amplitude of the first mode of the Fourier transform of the flame front is computed at each time step and tracked, providing the time evolution of the amplitude $A(t)$. The exponential growth rate ω is computed during the linear phase by:

$$\omega = \frac{\mathrm{d}}{\mathrm{d}t}\left[\ln(A(t))\right] \tag{19}$$

Care is taken to verify that the linear phase is well captured, as verified by the existence of a plateau at small times (between 0 and $\approx 6\ \tau$ in Fig. 1(c)) for ω as a function of time. The dispersion relation $\omega(k)$ is then obtained as a function of the wave number k as the procedure is repeated for different domain lengths. The numerical setup and operation for the dispersion relation extraction are described in Fig. 1. To validate the methodology, it was first applied to a pure H_2 air, $\phi = 0.5$ case and compared to the results of Berger et al. [21] and Frouzakis et al. [22] in Fig. 2. Good agreement with Frouzakis et al. [22] is obtained, whereas, at large wave numbers, a small deviation is observed with results from Berger et al. [21]. These small differences are likely due to different chemistry, transport properties, and DNS code.

3. Linear regime: linear stability analysis

3.1. Analyses of DNS database

At low equivalence ratio, characteristics of thermo-diffusive instabilities are recovered: super adiabaticity and higher heat release captured in positive curvature zones (i.e., zones where velocity streamlines are convex towards burned gases) than in negative curvature zones (i.e., zones where velocity streamlines are concave towards burned gases) as observed in Fig. 3 for pure H_2 cases at different equivalence ratios and Fig. 4 for an equivalence ratio of 0.4 at different NH_3 to H_2 ratios in the fuel. This was observed for lean pure H_2 by Howarth and Aspden [50], but we also observe this for lean NH_3/H_2 mixtures. The dispersion relations obtained by DNS are presented for different equivalence ratios and fuel compositions (Fig. 5) and pressure variations (Fig. 6). The symbols are the growth rate computed numerically for each domain size. A second-order polynomial fit of the growth rates is also plotted. Non-dimensionalized units of the growth rate versus the wave number ($\omega\tau$ versus $k\delta_L^0$) are used for all plots.

As expected, for all cases, $\omega\tau$ grows due to the destabilization of small wave numbers induced by hydrodynamic instabilities. Then $\omega\tau$ decreases for larger wave numbers $k\delta_L^0$ due to

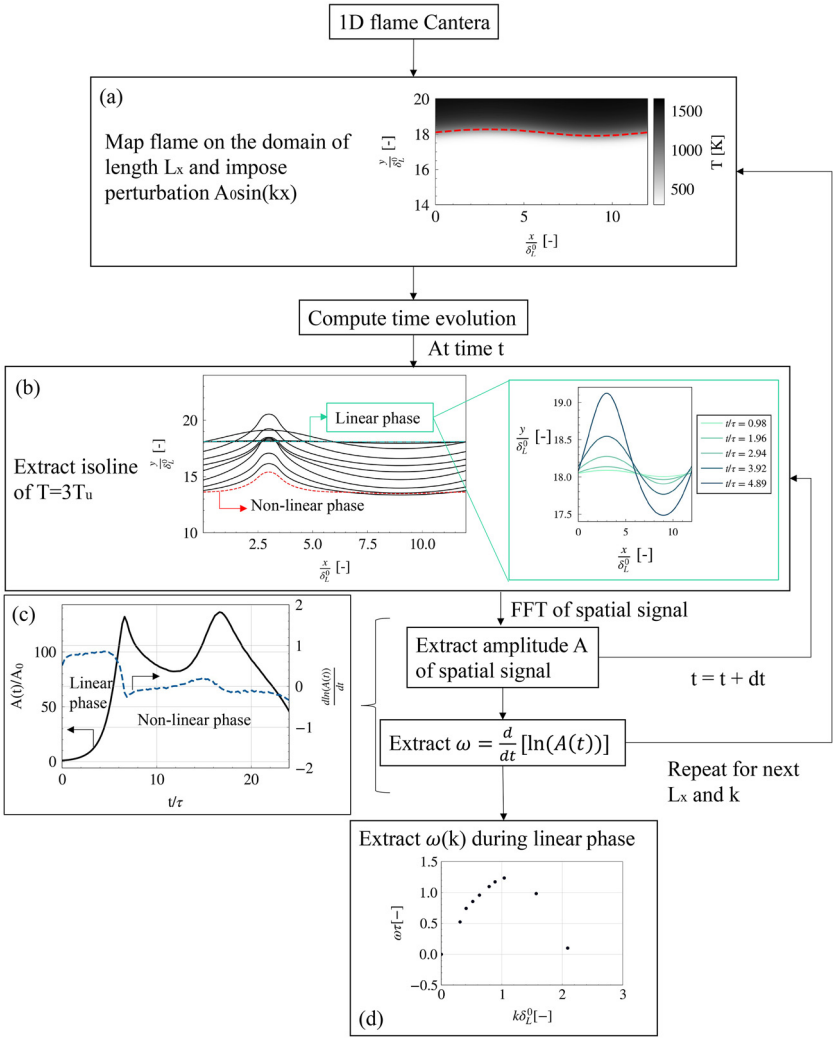

Fig. 1. Flowchart of the set up description and the extraction of $\omega(k)$.

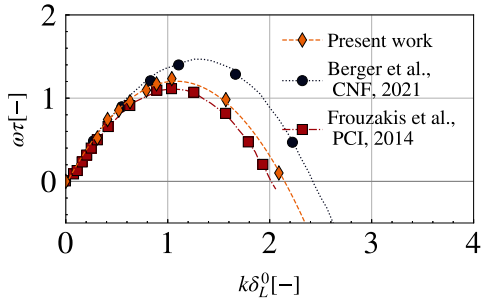

Fig. 2. Dispersion relation obtained in the methodology of Fig. 1 compared to the work by Berger et al. [21], and Frouzakis et al. [22] for pure H_2 at $\phi = 0.5$ and 1 bar.

thermo-diffusive effects within the flame front. To appreciate the effect of the hydrodynamic stability limit, $\omega_{DL}\tau$ as a function of the wave number is also plotted on the same figures for each mixture. A nearly constant expansion ratio for each fuel mixture at a given equivalence ratio leads to $\omega_{DL}\tau$ being almost superimposed.

For small wave numbers, cases at $\phi = 0.4$ have $\omega\tau$ exceeding $\omega_{DL}\tau$ which indicates that the contribution of the thermo-diffusive instability is to make the mixture more unstable (positive contribution of thermo-diffusive instabilities). On the other hand, at $\phi = 1.0$, the negative contribution of thermo-diffusive effects is observed since $\omega\tau$ are all below $\omega_{DL}\tau$. At 1 bar, the most unstable mixture ($\omega_{\max}\tau$ shown in Fig. 7(c)) corresponds to pure hydrogen at $\phi = 0.4$, with a maximum growth rate of more than twice that of $\phi = 1.0$. Figure 5 shows that the maximum growth rate obtained in the simulations diminishes with increasing equivalence ratio regardless of the fuel composition. This indicates the propensity of leaner mixtures to be more thermo-diffusely unstable, likely due to the small effective Lewis number of the mixture, indicating preferential diffusion. This had been observed by Berger et al. [21] and Frouzakis et al. [22] in the case of pure hydrogen. Figure 5 shows that these findings can be generalized for lean NH_3/H_2 flames. In Fig. 7, where the normalized maximum growth rate of each mixture is reported, we see that thermo-diffusive instabilities are reduced when the NH_3 content in the fuel increases at any given equivalence ratio, with a collapse of peak growth rate for all cases at stoichiometry.

Regarding the effects of pressure, Fig. 6 indicates a larger growth rate for 10 bar in the case of pure H_2 at $\phi = 0.5$ compared to 1 bar, as observed by Berger et al. [21] and Attili et al. [51] for CH_4. The same trend is found for the NH_3/H_2 case experimentally by Li et al. [27]. This is caused by both the thinner flame causing more instabilities at high pressure and the enhanced reactivity. Consistent in our simulations, ammonia addition makes the flame more stable than the pure hydrogen case at high pressure. These results also highlight the importance of pressure on instability dependency and should be considered for pressurized engine-like conditions.

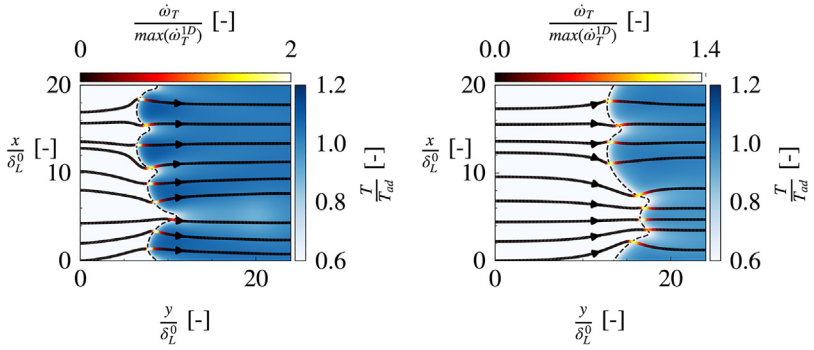

(a) X_{NH_3} : 0%, $\phi = 0.4$, $t/\tau \approx 10$

(b) X_{NH_3} : 0%, $\phi = 0.5$, $t/\tau \approx 15$

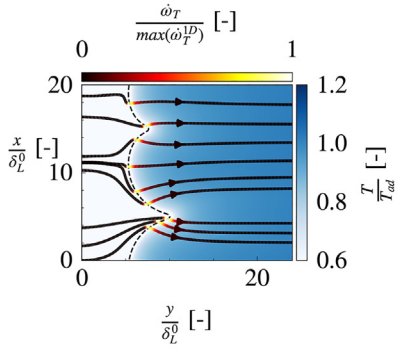

(c) X_{NH_3} : 0%, $\phi = 1.0$, $t/\tau \approx 40$

Fig. 3. Contour of normalized temperature, isocontour of temperature of $T = 3T_u$ in dashed lines, and velocity streamlines in solid lines colored by normalized heat release rate. Snapshots are taken at $t/\tau \approx 10$, 15, and 40 in the right column. Pure H_2 cases $\phi = 0.4$, 0,5 and 1.0.

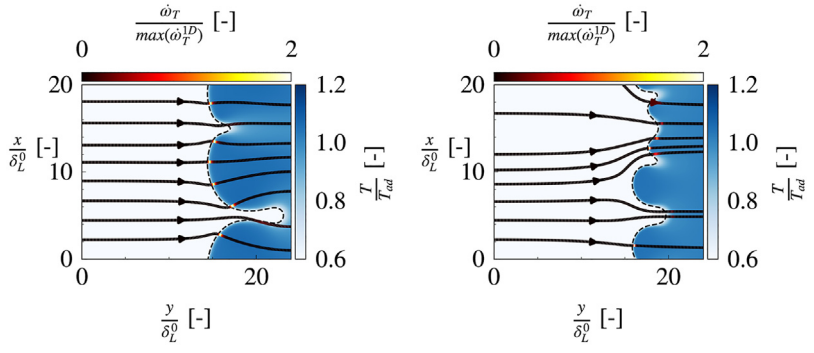

(a) X_{NH_3} : 30%, $\phi = 0.4$, $t/\tau \approx 5$

(b) X_{NH_3} : 50%, $\phi = 0.4$, $t/\tau \approx 5$

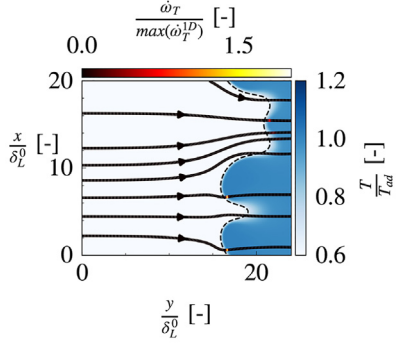

(c) X_{NH_3} : 60%, $\phi = 0.4$, $t/\tau \approx 5$

Fig. 4. Contour of normalized temperature, isocontour of temperature of $T = 3T_u$ in dashed lines, and velocity streamlines in solid lines colored by normalized heat release rate. Due to the slower flame speed, snapshots are taken at $t/\tau \approx 5$ in the right column. Mixtures with 30%, 50%, and 60% for $\phi = 0.4$.

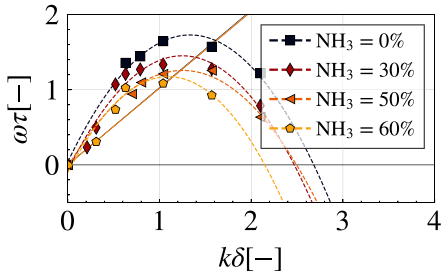

(a) $\phi = 0.4$

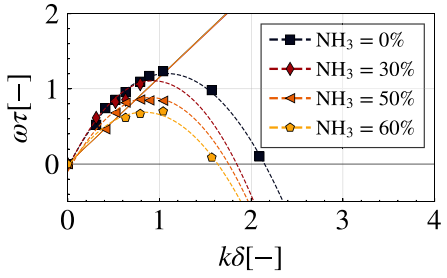

(b) $\phi = 0.5$

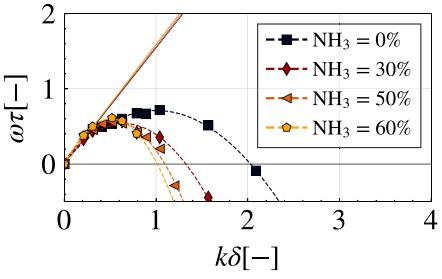

(c) $\phi = 1.0$

Fig. 5. Dispersion relation for varying equivalence ratio, at various NH_3 contents in volume in the fuel. Symbols correspond to the growth rates extracted from the simulations, dashed lines correspond to the second-order polynomial fit of these growth rates. The theoretical hydrodynamic growth rate $\omega_{DL}\tau$ is also shown in solid line for all mixtures.

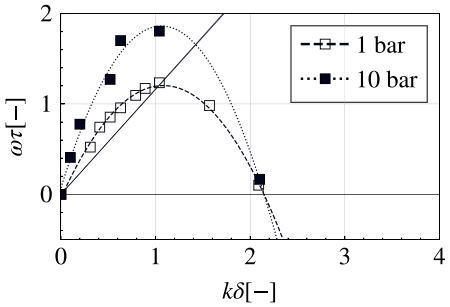

(a) X_{NH_3} : 0%, $\phi = 0.5$

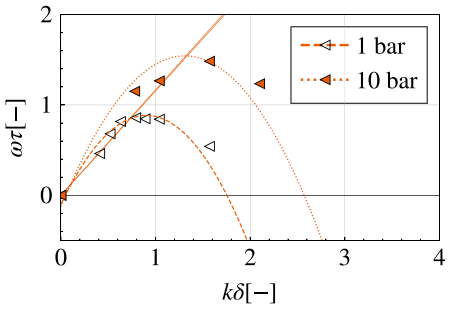

(b) X_{NH_3} : 50%, $\phi = 0.5$

Fig. 6. Dispersion relation for varying pressures, for NH_3 at 0% and 50% content in volume in the fuel at $\phi = 0.5$. Symbols correspond to the growth rates extracted from the simulations, dashed lines correspond to the second-order polynomial fit of the growth rates of cases at 1 bar, and the dotted lines to the growth rates with at 10 bar. The theoretical hydrodynamic growth rate $\omega_{DL}\tau$ is also shown in solid line for all mixtures.

A cut-off wavelength λ_c (Fig. 7(a) and (d)) associated with the cut-off wavenumber k_c where $\omega\tau$ become negative can be obtained from Figs. 5, 6. The normalized maximum growth rate $\omega_{\max}\tau$ (Fig. 7(c) and (f)) and the wavelength associated with the maximum growth rate $\lambda_{\omega_{\max}}$ (Fig. 7(b) and (e)), are also reported. The scaling of the critical wavelength λ_c and of $\lambda_{\omega_{\max}}$ depends directly on the flame thickness evolution δ_L^0. Finally, the dispersion relation of NH_3/H_2 mixtures evolves in a similar manner with equivalence ratio and pressure as pure H_2. NH_3 reduces the peak growth rate and, by extension, the instabilities for the investigated range of fuel content and equivalence ratio. We highlight that potentially, some proportions of ammonia and hydrogen could cause dissociation of ammonia into hydrogen, therefore leading to more instabilities, but that is not captured in the early linear phase of the flame front evolution and the peak growth rate increases with H_2 content in these cases.

3.2. Evaluation of Lewis number for NH_3/H_2 blends

For model development, finding global flame parameters to predict thermo-diffusive instabilities and computing theoretical relation dispersion instead of performing parametric sweeps with DNS would be preferred to limit the computational cost. However, these theoretical expressions still need to be verified and validated. For these compositions of ammonia/hydrogen, as discussed in Section 2, a suited definition for the effective Lewis number of a fuel blend needs to be evaluated. To do so, Cantera simulations of premixed, slightly strained flames are performed to compute the Markstein length [52] of the mixtures at different equivalence ratios. In these twin flames simulations, the premixed flame is obtained with a counterflow of two streams of fresh gases going against one another, leading to a strained flame [53]. This is done for the cases at 1 bar only. We compute the strain $\kappa = 2\dot{m}_u/\rho_u/w$ ($\dot{m}_u$ is the mass flow rate of the reactants and w the domain width between the two streams) and the flame consumption speed s_c in order to compute the Markstein length at small strains [54,55]:

$$L_b = \frac{s_l^0 - s_c}{\kappa}. \tag{20}$$

A negative (positive) value of the Markstein number, typically indicates an unstable (stable) mixture. Theoretical relations [54–56] link the Markstein length to global flame parameters: σ, β, x, λ and Le_{eff} which were defined in Section 2 :

$$Ma = \frac{L_b}{\delta_D} = \frac{\beta\,(Le_{\text{eff}} - 1)}{2(\sigma - 1)} \int_1^{\sigma} \frac{\bar{\lambda}(x)}{x} \ln\frac{\sigma - 1}{x - 1} dx. \tag{21}$$

By comparing the Markstein length from Cantera simulation with Eq. (21), it is possible to evaluate the best definition of the Lewis number. This is shown in Fig. 8 for three fuel compositions (30, 50 and 60% of NH_3) at atmospheric pressure. For the case with 30% NH_3, the strained Markstein length (20) is closest to the Markstein derived with the volume-based definition of the Lewis number (Le_V) compared to the other definitions. At 50% NH_3, the results from equivalence ratio 0.6 to 1 match very well the results using Le_V. Finally, the results for 60% NH_3 for the strained flame are between the volume-based definition (Le_V) and the diffusion-based definition (Le_D). Eq. (21) was derived for constant viscos-

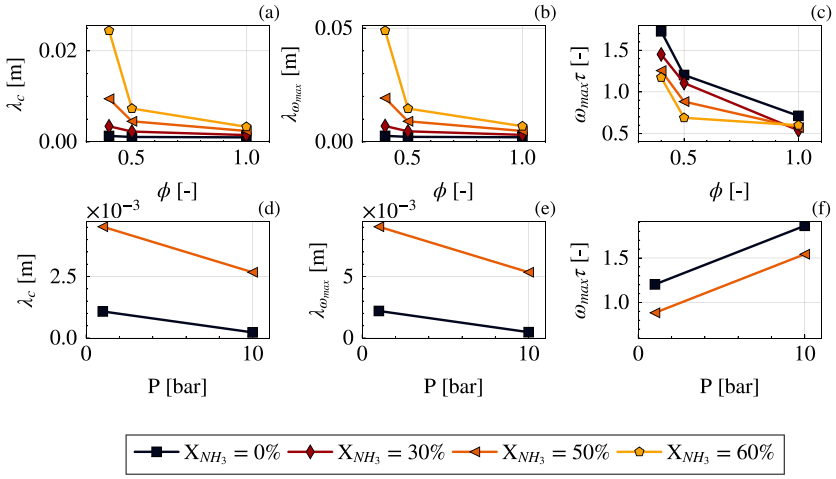

Fig. 7. Variation of the cut-off wavelength λ_c, the wavelength associated with the peak growth rate $\lambda_{\omega_{\max}}$, and the peak growth rate $\omega_{\max}\tau$. Top: Variation of equivalence ratio ϕ for different NH_3 fuel ratios. Bottom: Effect of initial pressure P for different NH_3 fuel ratios at equivalence ratio $\phi = 0.5$.

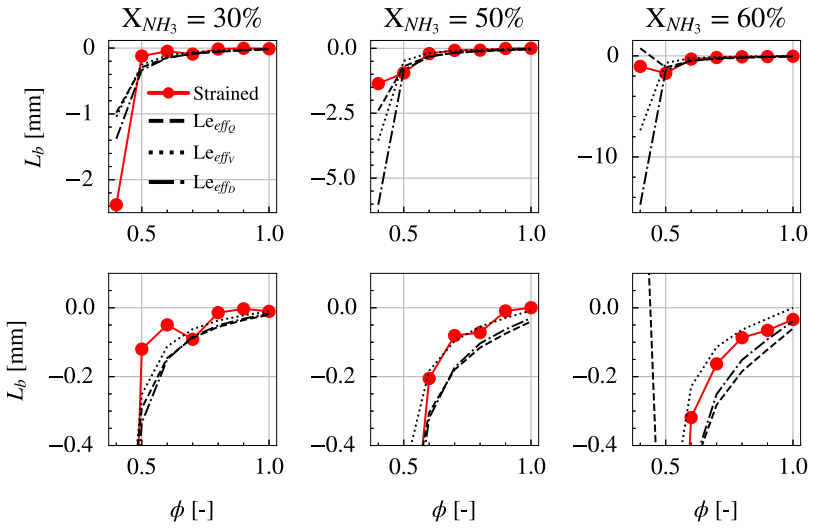

Fig. 8. Markstein length derived from Eq. (20) compared with Eq. (21) using different effective Lewis number definitions based on Le_Q, Le_V and Le_D. Top: full data points, bottom: a zoom on the y-axis to determine the most suited Lewis number definition.

ity with single-step flame, where the Zel'dovich number β was also derived with assumptions to compute the activation energy. Therefore, the computation of the theoretical formulas for β and L_b leads to uncertainty in the results to compare the Lewis numbers. We also note that at a low equivalence ratio ($\phi = 0.4$), the strained-derived Markstein number is not well reproduced with any of the Lewis definitions in the theoretical relation (21). Here we suggest that, among all the investigated definitions, Le_V best captures, overall, the instabilities of the mixtures compared to the other definitions for the NH_3/H_2 mixture for different equivalence ratios in lean to stoichiometric cases. This is a similar conclusion reached by Zitouni et al. [29] for a large range of equivalence ratio and NH_3/H_2 ratio.

3.3. Comparison of DNS-derived relation dispersion with theoretical dispersion relations

The Lewis number definition Le_V (Eq. (14)) based on volume is then used in the theoretical dispersion relations of Sivashinsky Eq. (12) and Matalon's Eq. (6). We present the results for the three equivalence ratios in this study $\phi = 0.4$, 0.5, and 1, and for the cases with pure H_2 and 50% of NH_3. The relation dispersions for $\phi = 0.4$, 0.5, and 1 for all fuel contents are presented in the Supplementary Materials in Fig. B.1.

Matalon's theory [16] captures the stabilizing effect of large wave numbers for very large values of k for cases $\phi = 0.4$ and 0.5, not seen on the figure due to the x-axis limit. Large deviations from the DNS-derived dispersion relation are found, with the cut-off wavelength and the peak growth rate not reproduced with the two theoretical relation dispersions. This is true for leaner cases since Matalon's relation for the stoichiometric case leads to a closer cut-off wavelength and peak growth rate to the DNS results. The model by Sivashinsky [19] predicts the stabilizing effects at high wave numbers thanks to the inclusion of the fourth-order term. For all cases, the cut-off wavelength and peak growth rate are not well evaluated compared to the DNS results due to density variation throughout the flame front not being included in Sivashinsky's model. Section 3.2 showed the difficulty of the mixture's Lewis number definitions to reproduce the Markstein at these low equivalence ratios. We find that theoretical formulas for the dispersion relation also struggle to match results with DNS for pure H_2 for which the Lewis number definition is well defined. This suggests that these theories are not able to capture the flame behavior at a low equivalence ratio, even if the Lewis number is

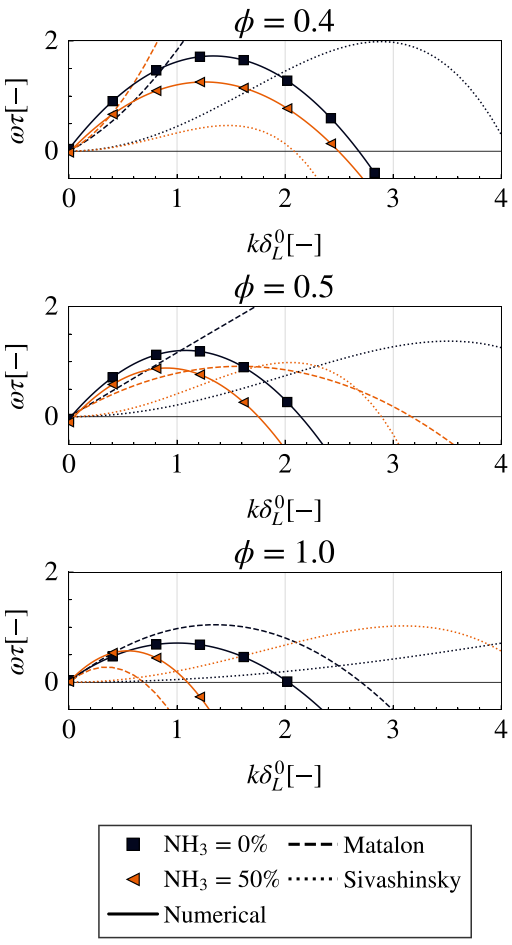

Fig. 9. Computed dispersion relation (solid line with symbol) compared with theoretical dispersion relation using the volume-based definition of the Lewis number: Matalon's dispersion relation Eq. (6) (dashed line) and Sivashinsky's relation Eq. (12) (dotted line). ω_{DL} is not pictured as it was already in Fig. 5. Case $\phi = 0.4$, 0.5 and 1 for 0% NH_3 and 50% NH_3.

not well defined at small equivalence ratios. Overall, these results indicate a need for theoretical dispersion relations to account for preferential diffusion effects occurring at small equivalence ratios to be suited for H_2 and mixtures of NH_3/H_2 (Fig. 9).

3.4. Impact of Zel'dovich number and expansion ratio

To assess the impact of ammonia addition on other global flame parameters, and understand its stabilizing effect seen in Section 3, Fig. 10 presents the values obtained from one-dimensional Cantera simulation for the unstretched laminar velocity, Zel'dovich number, and expansion ratio -defined Section 2- to measure the impact of these global parameters on the instabilities. We consider both cases at 1 and 10 bar. The laminar flame speed increases with equivalence ratio up to stoichiometry and increases with the hydrogen content in the fuel. At $\phi = 0.5$, the pressure increase results in a decrease of s_L^0. Lower values of the Zel'dovich number indicate a stronger reactivity. Higher H_2 contents lead to a lower Zel'dovich number: ammonia addition lessens the reactivity of the mixtures. Zel'dovich number decreases with increasing equivalence ratio indicating higher reactivity towards stoichiometry as captured by higher adiabatic temperatures. The similar Zel'dovitch number at $\phi = 1.0$ for all fuel blends can explain the collapse of the peak growth rate observed Fig. 7. The higher pressure leads to a thinner flame thickness and a lower flame speed, leading to more instabilities. However, based on the δ_L^0 evolution with pressure, compared with the evolution of λ_c from Fig. 7 with pressure, we can conclude that the pressure effect on the flame thickness and flame speed is not the only reason for the instability increase (if it had been, the evolution for both quantities would have been proportional, which it is not the case here for both H_2 and NH_3/H_2). Therefore, there are two mechanisms due to pressure: the instabilities increase due to the thinner flame, but the domination of chain termination reaction and the increase of reactivity also leads to larger instabilities. Indeed, the Zel'dovich number increases as we shift towards high pressure for both the pure H_2 case and the 50% of NH_3 case. Increasing the Zel'dovich number for increasing pressure is found for H_2 and NH_3/H_2 flames due to chain termination reactions becoming more important at high pressure than chain branching reactions. The domination of chain termination reactions leads to a higher temperature at higher pressure, as seen in Table 1 and to a more reactive mixture. This was also found for pure methane by Attili et al. [51]. The fuel mixture does not strongly affect the expansion ratio at a given equivalence ratio, but a larger difference appears at stoichiometry. Indeed, as the equivalence ratio increases, H_2O formation increases, leading to a large difference in density between burned and unburned gases. And as the ammonia content increases in the fuel, NO formation increases, leading to a larger unbalance between burned and unburned gas

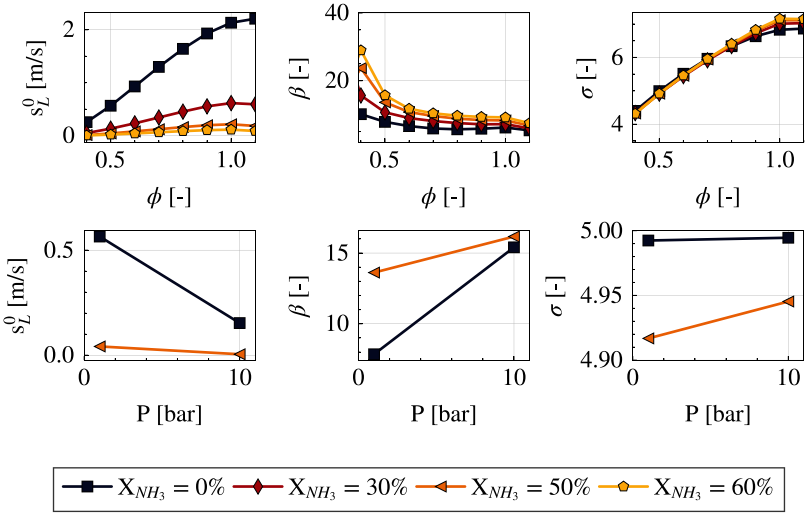

Fig. 10. Variation of laminar unstretched flame speed s_L^0, Zel'dovich number β, and expansion ratio σ. Top: variation of equivalence ratio ϕ for different NH_3 fuel ratios. Bottom: Variation of initial pressure P for different NH_3 fuel ratios at equivalence ratio $\phi = 0.5$.

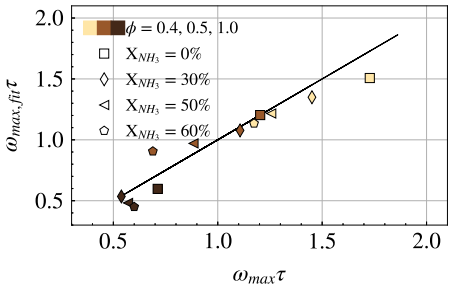

Fig. 11. Fit for $\omega_{\max}\tau$ based on ϕ and X_{NH_3}.

densities. The influence of pressure on the expansion ratio is minimal.

Overall, ammonia addition in the fuel leads to a higher expansion ratio due to more products exacerbating the density difference between burned and unburned gases. Furthermore, ammonia addition reduces reactivity, reducing the Zel'dovitch number. The dispersion relation and peak growth rate are impacted by these different parameters, as well as by the effective Lewis number, as they change with mixture composition, equivalence ratio, and pressure and impact the reactivity, hydrodynamic stability, and preferential diffusion.

3.5. Fit for $\omega_{\max}\tau$ for atmospheric conditions

DNS data can be used to suggest a fit based on the mixture composition for atmospheric conditions to estimate the value of $\omega_{\max}\tau$ for various NH_3/H_2 compositions at different equivalence ratios. This is similar to what Berger et al. [21] did for pure H_2 and Attili et al. [51] for CH_4. Eq. (22) is derived from the observed DNS results to assess the impact of fuel content and equivalence ratio and can be used to estimate criterion for thermo-diffusive instabilities importance such as the ones suggested by Chomiak and Lipatnikov [57] and Chaudhuri et al. [58]. It can also be useful for modeling purposes to suggest such an empirical fit [21,50,59,60]. The fit is based on the composition ϕ and fuel content X_{NH_3}, and is suited only for atmospheric conditions:

$$\omega_{\max,fit}\tau = \omega_{\max,ref}\tau \left(\frac{\phi}{\phi_{ref}}\right)^{a} \left(\frac{(1-X_{NH_3})}{(1-X_{NH_3})_{ref}}\right)^{b} \tag{22}$$

with $a = -1.01$ and $b = 0.31$. Results (Fig. 11) show the fit's accuracy and indicate that an equivalence ratio increase will lead to a lower peak growth rate while an increase of X_{NH_3} will lead to a lower peak growth rate.

4. Conclusion

The dispersion relations of an extensive dataset of NH_3/H_2/air premixed flames, with varying fuel ratios of hydrogen and ammonia, equivalence ratio, and pressure were numerically computed through high fidelity Direct Numerical Simulations. The dispersion relations were extracted from growth rate computation for varying initial wavelength perturbation. This allowed studying the effects of intrinsic instabilities on the flame front. The study leads to the following findings:

- Darrieus–Landau instabilities were found to dominate mixtures at stoichiometry, and the computed relation dispersion relation was equal to or below the Darrieus–Landau dispersion relation for all wave numbers: the thermo-diffusive mechanisms has no impact on the mixture. On the other hand, for leaner mixtures, the computed dispersion relation is above the Darrieus–Landau dispersion relation at small wave numbers: the thermo-diffusive mechanism has a positive impact on the mixture.
- An investigation of slightly strained flames has been performed to select a Lewis number definition that can be used in theoretical relations. We find the volume-based Lewis number (Le_V) to be best suited for NH_3/H_2 mixtures.
- Comparisons with theoretical dispersion relations showed the theory's difficulty in fitting the stabilizing effects at large wave numbers for lean mixtures. This indicates a need for new theoretical relations to capture lean flames behavior. This was known for pure hydrogen but is now extended to mixtures of ammonia and hydrogen.
- Within the investigated range of operating points, we use quantitative arguments to show that ammonia addition leads to more stable mixtures. The impact of ammonia dissociating into hydrogen and leading to an increase of instabilities has not been captured in this work, but it would be interesting to investigate a larger amount of operating conditions to see if, in some cases, ammonia addition might actually lead to more instability. However, the investigation of more operating conditions is outside of the scope of this study.
- Higher peak growth rates were computed for leaner mixtures, indicating that leaner flames are more unstable, even for NH_3/H_2 mixtures.
- A pressure increase resulted in a higher growth rate as chain termination reactions became more important for both NH_3/H_2 mixtures and pure H_2.

Concluding, the present study contributes to the fundamental understanding of ammonia/hydrogen combustion and the development of thermo-diffusive effects. Furthermore, it provides unique correlations and datasets that could be used for modeling purposes following what is proposed for pure hydrogen-air flames by Berger et al. [21,59] and Aniello et al. [60].

Declaration of Competing Interest

The authors declare that they have no known competing financial interests or personal relationships that could have appeared to influence the work reported in this paper.

Acknowledgments

The Authors gratefully acknowledge the support from the Norwegian Research Council (296207) and related partners in the Low Emission Centre. This project has received funding from the European Research Council under the European Union's Horizon 2020 research and innovation program Grant Agreement 832248, SCIROCCO. The computations were performed on resources provided by Sigma2 - the National Infrastructure for High-Performance Computing and Data Storage in Norway (project nn9527k), on the BETZY supercomputer, and of GENCI-TGCC under grant agreement n° 2023-A0132B10157. CERFACS provided the software AVBP, and technical support for the software was provided by Dr. O. Vermorel and Dr. G. Staffelbach. Dr. A. Gruber is also acknowledged for providing computational resources and technical support. A. Coudray is acknowledged for the reduction of the kinetic mechanism used in this study. J.-J. Hok and N. Detomaso are also acknowledged for insightful discussion into the Markstein length definitions.

Supplementary material

Supplementary material associated with this article can be found, in the online version, at doi:10.1016/j.combustflame.2023.112986.

References

[1] F.W. Taylor, The greenhouse effect and climate change revisited, Rep. Prog. Phys. 65 (2001) 1.
[2] I. Staffell, D. Scamman, A. Velazquez Abad, P. Balcombe, P.E. Dodds, P. Ekins, N. Shah, K.R. Ward, The role of hydrogen and fuel cells in the global energy system, Energy Environ. Sci. 12 (2019) 463–491.
[3] D.R. MacFarlane, P.V. Cherepanov, J. Choi, B.H. Suryanto, R.Y. Hodgetts, J.M. Bakker, F.M. Ferrero Vallana, A.N. Simonov, A roadmap to the ammonia economy, Joule 4 (2020) 1186–1205.
[4] H. Kobayashi, A. Hayakawa, K. Somarathne, E. Okafor, Science and technology of ammonia combustion, Proc. Combust. Inst. 37 (2019) 109–133.
[5] A. Valera-Medina, F. Amer-Hatem, A.K. Azad, I.C. Dedoussi, M. de Joannon, R.X. Fernandes, P. Glarborg, H. Hashemi, X. He, S. Mashruk, J. McGowan, C. Mounaim-Rouselle, A. Ortiz-Prado, A. Ortiz-Valera, I. Rossetti, B. Shu, M. Yehia, H. Xiao, M. Costa, Review on ammonia as a potential fuel: from synthesis to economics, Energy Fuels 35 (2021) 6964–7029.
[6] H.G. Im, J.H. Chen, Preferential diffusion effects on the burning rate of interacting turbulent premixed hydrogen-air flames, Combust. Flame 131 (2002) 246–258.
[7] H.C. Lee, P. Dai, M. Wan, A.N. Lipatnikov, Lewis number and preferential diffusion effects in lean hydrogen–air highly turbulent flames, Phys. Fluids 34 (2022) 035131.
[8] P. Ahmed, B. Thorne, M. Lawes, S. Hochgreb, G.V. Nivarti, R.S. Cant, Three dimensional measurements of surface areas and burning velocities of turbulent spherical flames, Combust. Flame 233 (2021) 111586.
[9] M.S. Wu, S. Kwon, J.F. Driscoll, G.M. Faeth, Turbulent premixed hydrogen/air flames at high Reynolds numbers, Combust. Sci. Technol. 73 (1990) 327–350.
[10] L. Berger, A. Attili, H. Pitsch, Synergistic interactions of thermo-diffusive instabilities and turbulence in lean hydrogen flames, Combust. Flame 244 (2022) 112254.
[11] A. Aspden, M. Day, J. Bell, Turbulence-chemistry interaction in lean premixed hydrogen combustion, Proc. Combust. Inst. 35 (2015) 1321–1329.
[12] W. Song, F.E. Hernández-Pérez, H.G. Im, Diffusive effects of hydrogen on pressurized lean turbulent hydrogen-air premixed flames, Combust. Flame 246 (2022) 112423.
[13] S. Wiseman, M. Rieth, A. Gruber, J.R. Dawson, J.H. Chen, A comparison of the blow-out behavior of turbulent premixed ammonia/hydrogen/nitrogen-air and methane-air flames, Proc. Combust. Inst. 38 (2021) 2869–2876.
[14] V. Coulon, J. Gaucherand, V. Xing, D. Laera, C. Lapeyre, T. Poinsot, Direct numerical simulations of methane, ammonia-hydrogen and hydrogen turbulent premixed flames, Combust. Flame 256 (2023) 112933.
[15] M. Rieth, A. Gruber, F.A. Williams, J.H. Chen, Enhanced burning rates in hydrogen-enriched turbulent premixed flames by diffusion of molecular and atomic hydrogen, Combust. Flame 239 (2022) 111740.
[16] M. Matalon, B.J. Matkowsky, Flames as gasdynamic discontinuities, J. Fluid Mech. 124 (1982) 239–259.
[17] P. Pelce, P. Clavin, Influence of hydrodynamics and diffusion upon the stability limits of laminar premixed flames, J. Fluid Mech. 124 (1982) 219–237.
[18] P. Clavin, J.C. Graña-Otero, Curved and stretched flames: the two Markstein numbers, J. Fluid Mech. 686 (2011) 187–217.
[19] G.I. Sivashinsky, Instabilities, pattern formation, and turbulence in flames, Annu. Rev. Fluid Mech. 15 (1983) 179–199.
[20] G.I. Sivashinsky, Diffusional-thermal theory of cellular flames, Combust. Sci. Technol. 15 (3–4) (1977) 137–145.
[21] L. Berger, A. Attili, H. Pitsch, Intrinsic instabilities in premixed hydrogen flames: parametric variation of pressure, equivalence ratio, and temperature. Part 1 - dispersion relations in the linear regime, Combust. Flame 240 (2022) 111935.
[22] C.E. Frouzakis, N. Fogla, A.G. Tomboulides, C. Altantzis, M. Matalon, Numerical study of unstable hydrogen/air flames: shape and propagation speed, Proc. Combust. Inst. 35 (2015) 1087–1095.
[23] C. Altantzis, C. Frouzakis, A. Tomboulides, S. Kerkemeier, K. Boulouchos, Detailed numerical simulations of intrinsically unstable two-dimensional planar lean premixed hydrogen/air flames, Proc. Combust. Inst. 33 (2011) 1261–1268.
[24] J. Yuan, Y. Ju, C.K. Law, On flame-front instability at elevated pressures, Proc. Combust. Inst. 31 (2007) 1267–1274.
[25] J. Yu, R. Yu, X. Bai, M. Sun, J. Tan, Nonlinear evolution of 2D cellular lean hydrogen/air premixed flames with varying initial perturbations in the elevated pressure environment, Int. J. Hydrog. Energy 42 (2017) 3790–3803.
[26] J. Lee, S. Lee, O. Kwon, Effects of ammonia substitution on hydrogen/air flame propagation and emissions, Int. J. Hydrog. Energy 35 (2010) 11332–11341.
[27] Y. Li, M. Bi, B. Li, Y. Zhou, L. Huang, W. Gao, Explosion hazard evaluation of renewable hydrogen/ammonia/air fuels, Energy 159 (2018) 252–263.
[28] A. Ichikawa, A. Hayakawa, Y. Kitagawa, K.K.A. Somarathne, T. Kudo, H. Kobayashi, Laminar burning velocity and Markstein length of ammonia/hydrogen/air premixed flames at elevated pressures, Int. J. Hydrog. Energy 40 (30) (2015) 9570–9578.
[29] S. Zitouni, P. Brequigny, C. Mounaim-Rousselle, Influence of hydrogen and methane addition in laminar ammonia premixed flame on burning velocity, Lewis number and Markstein length, Combust. Flame 253 (2023) 112786.
[30] G. Darrieus, Propagation d'un front de flamme, Tech. Mod. 30 (1938) 18.
[31] L. Landau, On the theory of slow combustion, in: P. Pelcé (Ed.), Dynamics of Curved Fronts, Academic Press, San Diego (1988), pp. 403–411.
[32] M. Matalon, C. Cui, J.K. Bechtold, Hydrodynamic theory of premixed flames: effects of stoichiometry, variable transport coefficients and arbitrary reaction orders, J. Fluid Mech. 487 (2003) 179–210.
[33] C. Sun, C. Sung, L. He, C. Law, Dynamics of weakly stretched flames: quantitative description and extraction of global flame parameters, Combust. Flame 118 (1999) 108–128.
[34] G. Sivashinsky, Nonlinear analysis of hydrodynamic instability in laminar flames—I. Derivation of basic equations, Acta Astronaut. 4 (11–12) (1977) 1177–1206.
[35] A.Y. Klimenko, A.G. Class, On premixed flames as gasdynamic discontinuities: asimple approach to derive their propagation speed, Combust. Sci. Technol. 160 (2000) 23–33.
[36] S. Chung, C. Law, An integral analysis of the structure and propagation of stretched premixed flames, Combust. Flame 72 (1988) 325–336.
[37] A. Lipatnikov, J. Chomiak, Molecular transport effects on turbulent flame propagation and structure, Prog. Energy Combust. Sci. 31 (2005) 1–73.
[38] G. Joulin, T. Mitani, Linear stability analysis of two-reactant flames, Combust. Flame 40 (1981) 235–246.
[39] D. Lapalme, R. Lemaire, P. Seers, Assessment of the method for calculating the Lewis number of H_2/CO/CH_4 mixtures and comparison with experimental results, Int. J. Hydrog. Energy 42 (2017) 8314–8328.
[40] N. Bouvet, F. Halter, C. Chauveau, Y. Yoon, On the effective Lewis number formulations for lean hydrogen/hydrocarbon/air mixtures, Int. J. Hydrog. Energy 38 (2013) 5949–5960.
[41] S. Muppala, M. Nakahara, N. Aluri, H. Kido, J. Wen, M. Papalexandris, Experimental and analytical investigation of the turbulent burning velocity of two–component fuel mixtures of hydrogen, methane and propane, Int. J. Hydrog. Energy 34 (2009) 9258–9265.
[42] F. Dinkelacker, B. Manickam, S. Muppala, Modelling and simulation of lean premixed turbulent methane/hydrogen/air flames with an effective Lewis number approach, Combust. Flame 158 (2011) 1742–1749.
[43] C. Law, G. Jomaas, J. Bechtold, Cellular instabilities of expanding hydrogen/propane spherical flames at elevated pressures: theory and experiment, Proc. Combust. Inst. 30 (2005) 159–167.
[44] T. Schönfeld, M. Rudgyard, Steady and unsteady flow simulations using the hybrid flow solver AVBP, AIAA J. 37 (1999) 1378–1385.
[45] A. Stagni, C. Cavallotti, S. Arunthanayothin, Y. Song, O. Herbinet, F. Battin-Leclerc, T. Faravelli, An experimental, theoretical and kinetic-modeling study of the gas-phase oxidation of ammonia, React. Chem. Eng. 5 (2020) 696–711.
[46] Q. Cazères, P. Pepiot, E. Riber, B. Cuenot, A fully automatic procedure for the analytical reduction of chemical kinetics mechanisms for computational fluid dynamics applications, Fuel 303 (2021) 121247.
[47] P. Lax, B. Wendroff, Systems of conservation laws, Commun. Pure Appl. Math. 13 (1960) 217–237.
[48] D.G. Goodwin, H.K. Moffat, I. Schoegl, R.L. Speth, B.W. Weber, Cantera: an object-oriented software toolkit for chemical kinetics, thermo-dynamics, and transport processes, 2022. Version 2.6.0.
[49] T. Poinsot, S. Lelef, Boundary conditions for direct simulations of compressible viscous flows, J. Comput. Phys. 101 (1992) 104–129.
[50] T. Howarth, A. Aspden, An empirical characteristic scaling model for freely-propagating lean premixed hydrogen flames, Combust. Flame 237 (2022) 111805.
[51] A. Attili, R. Lamioni, L. Berger, K. Kleinheinz, P.E. Lapenna, H. Pitsch, F. Creta, The effect of pressure on the hydrodynamic stability limit of premixed flames, Proc. Combust. Inst. 38 (2021) 1973–1981.
[52] G.H. Markstein, Nonsteady Flame Propagation: AGARDograph, Elsevier, 2014.
[53] J. Buckmaster, D. Mikolaitis, The premixed flame in a counterflow, Combust. Flame 47 (1982) 191–204.
[54] T. Poinsot, D. Veynante, Theoretical and Numerical Combustion, Edwards, 2005.
[55] J. Bechtold, M. Matalon, The dependence of the Markstein length on stoichiometry, Combust. Flame 127 (1) (2001) 1906–1913.
[56] P. Clavin, G. Joulin, Premixed flames in large scale and high intensity turbulent flow, J. Phys. Lett. 44 (1) (1983).
[57] J. Chomiak, A.N. Lipatnikov, Simple criterion of importance of laminar flame instabilities in premixed turbulent combustion of mixtures characterized by low Lewis numbers, Phys. Rev. E 107 (2023) 015102.
[58] S. Chaudhuri, V. Akkerman, C.K. Law, Spectral formulation of turbulent flame speed with consideration of hydrodynamic instability, Phys. Rev. E 84 (2011) 026322.
[59] L. Berger, A. Attili, H. Pitsch, Intrinsic instabilities in premixed hydrogen flames: parametric variation of pressure, equivalence ratio, and temperature. Part 2 – non-linear regime and flame speed enhancement, Combust. Flame 240 (2022) 111936.
[60] A. Aniello, D. Laera, L. Berger, A. Attili, T. Poinsot, Introducing thermo-diffusive effects in large-eddy simulation of turbulent combustion for lean hydrogen-air flames, Proceedings of the 2022 Summer Program (2022).